Multicompartment Cascade Reactions

DOI: 10.1002/anie.201308141

Cascade Reactions in Multicompartmentalized Polymersomes**

Ruud J. R. W. Peters, Maïté Marguet, Sébastien Marais, Marco W. Fraaije, Jan C. M. van Hest, and Sébastien Lecommandoux**

Abstract: *Enzyme-filled polystyrene-b-poly(3-(isocyano-L-alanyl-aminoethyl)thiophene) (PS-b-PIAT) nanoreactors are encapsulated together with free enzymes and substrates in a larger polybutadiene-b-poly(ethylene oxide) (PB-b-PEO) polymersome, forming a multicompartmentalized structure, which shows structural resemblance to the cell and its organelles. An original cofactor-dependent three-enzyme cascade reaction is performed, using either compatible or incompatible enzymes, which takes place across multiple compartments.*

Compartmentalization is one of the key features developed by nature during the evolution of eukaryotic cells.[1,2] In fact, according to some of the leading theories, compartmentalization was even instrumental in the origin of life,[1] because in order to start an evolutionary process molecules should be kept close together to allow advantageous mutations to lead to preferential replication.[1] In recent years, a growing effort has been made to study cellular function by artificially mimicking or reconstructing (parts of) cells.[3,4] Single-compartment "minimal cells", which are lipid-based systems containing the minimal components necessary to be living,[5] have been created that are capable of DNA replication and protein production[6,7] or self-replication.[8]

Eukaryotic cells are, however, multicompartmentalized structures, in which smaller organelle compartments also reside inside the cell. Multicompartmentalization in eukaryotic cells allows the positional assembly and spatial separation of biomolecules and processes in different compartments inside the cell, which provides the cell with spatiotemporal control over metabolic reactions.[9] Confinement also leads to the possibility of spatially separating reaction pathways or incompatible components or of locally creating high amounts of reagents, or concentration gradients, to guide metabolic flux.[10,11] Examples of natural reaction pathways that involve multiple enzymes and substrate molecules and can take place in multiple successive cellular compartments are the Calvin cycle for carbon fixation[12] or the citric acid cycle, which takes place in mitochondria but interacts with many cytosolic pathways.[13]

Previously, a few different multicompartmentalized structures have been reported with the advent of the development of new microreactor architectures.[3] These structures were either based on a liposomes-in-liposome system[14] or on liposomes in layer-by-layer (LbL) capsules,[15–17] and only single enzyme reactions were described. Also, a concentric, two-compartment, LbL capsule-in-capsule architecture with a known two-enzyme cascade, based on glucose oxidase and horseradish peroxidase, has been reported.[18] Polymersomes are a third class of membrane-mimetic materials used for the construction of multicompartmentalized systems. These polymer-based vesicles offer several beneficial properties: good colloidal and mechanical stability, tailored permeability,[19] and stimuli responsiveness[20] or biodegradation.[21] On one hand, active enzymes can be trapped in semipermeable polymersomes that only allow the diffusion of small substrate molecules into their structure, which yields nanoreactors;[22–24] if these nanoreactors are incorporated into living cells, they function as "artificial organelles".[25–27] On the other hand, loading smaller polymersomes into the lumen of a larger one can create a polymersomes-in-polymersome system.[28–31]

Although already demonstrating some of the possibilities of multicompartmentalization, the aforementioned microencapsulated reactors, however, still do not possess the complexity required to mimic cellular reaction pathways that take place in multiple successive compartments.

Herein, we describe the combination of both the structural cell mimicry of polymersomes-in-polymersomes and the functional aspects of enzymatic polymersome nanoreactors as organelle mimics into a single system, in order to study the

[*] R. J. R. W. Peters,[+] Prof. J. C. M. van Hest
Radboud University Nijmegen
Institute for Molecules and Materials, Bio-organic Chemistry
Heyendaalseweg 135, 6525 AJ, Nijmegen (The Netherlands)
E-mail: j.vanhest@science.ru.nl

M. Marguet,[+] Prof. S. Lecommandoux
Université de Bordeaux, LCPO
UMR 5629, 33600 Pessac (France)
and
CNRS, LCPO
UMR 5629, 33600 Pessac (France)
E-mail: lecommandoux@enscbp.fr

S. Marais
Bordeaux Imaging Center Université Bordeaux Segalen
CNRS UMS3420—Inserm US004, Institut François Magendie
146 rue Léo-Saignat, 33077 Bordeaux Cedex (France)

Prof. M. W. Fraaije
University of Groningen
Biomolecular Sciences and Biotechnology Institute, Laboratory of Biochemistry
Nijenborgh 4, 9747 AG Groningen (The Netherlands)

[+] These authors contributed equally to this work.

[**] R.J.R.W.P. thanks the Dutch Science Foundation (NWO) for funding. M.M. and S.L. thank the French Ministère de l'Enseignement Supérieur et de la Recherche and the Precision Polymer Materials P2M program from the European Science Foundation for funding. J.C.M.v.H. acknowledges funding from the Ministry of Education, Culture and Science (Gravity program 024.001.035). M. van Eldijk is thanked for help with size-exclusion chromatography measurements.

Supporting information for this article is available on the WWW under http://dx.doi.org/10.1002/anie.201308141.

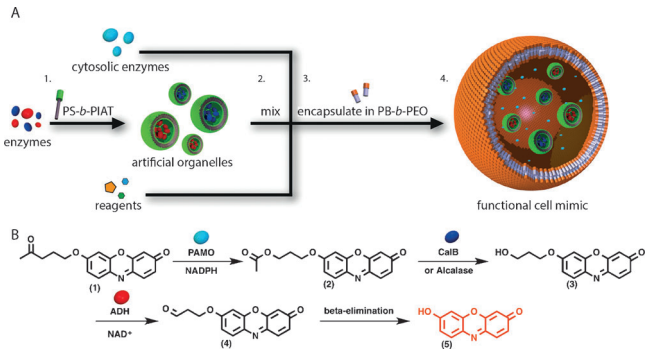

Figure 1. A) The concept of the cell mimic, which shows the initial encapsulation of different enzymes in polystyrene-*b*-poly(3-(isocyano-L-alanyl-amino-ethyl)-thiophene) (PS-*b*-PIAT) nanoreactors (1), followed by mixing of the organelle mimics, cytosolic enzymes, and reagents (2), before encapsulation of the reaction mixture in polybutadiene-*b*-poly(ethylene oxide) (PB-*b*-PEO) vesicles (3) to create the functional cell mimic (4), inside which enzymatic multicompartment catalysis takes place. B) Detailed cascade reaction scheme. Profluorescent substrate **1** undergoes a Baeyer–Villiger reaction catalyzed by phenylacetone monooxygenase (PAMO), with one unit of the reduced form of nicotinamide adenine dinucleotide phosphate (NADPH) being consumed, to yield ester **2**, which is subsequently hydrolyzed by *Candida antarctica* lipase B (CalB) or alcalase to provide primary alcohol **3**. Alcohol dehydrogenase (ADH) oxidizes the alcohol, by using the cofactor nicotinamide adenine dinucleotide (NAD^+), to give aldehyde **4**, which then undergoes spontaneous beta-elimination to yield resorufin (**5**) as the final fluorescent product.

effects of multicompartmentalization and confinement on cellular multistep reaction pathways (Figure 1 a). By placing the enzymes needed for each separate cascade step in different (sub)compartments, we aim to force the reaction intermediates to cross over compartmental boundaries. We thereby hope to observe truly confined reactions and the local or gradient-like generation of reaction products, as occurs in nature.

To demonstrate structural and functional control in a multicompartmentalized system, an original and complex multistep model reaction that resembles a natural enzymatic pathway, as depicted in Figure 1 b, was investigated. In this pathway, the profluorescent substrate **1** first undergoes oxidation by the solvent- and temperature-stable Baeyer–Villiger monooxygenase, PAMO,[32] which uses NADPH as a cofactor. The resulting ester moiety is then hydrolyzed by CalB, and subsequent oxidation of the resulting alcohol to an aldehyde is achieved by an NAD^+-dependent ADH. Finally, the last reaction yields fluorescent resorufin (**5**) through a nonenzymatic, but spontaneous, beta-elimination step. In particular, the use of cofactors like NADPH and NAD^+ as electron donors or acceptors in enzymatic reactions is very common in nature.[33]

For the development of the synthetic organelles, enzymes involved in the cascade reaction were encapsulated in intrinsically porous, sub-micrometric PS_{40}-*b*-$PIAT_{50}$ nanoreactors.[22] The PS-*b*-PIAT nanoreactors, cytosolic enzymes, and reaction components were then quantitatively[34] encapsulated in micrometer-sized PB-*b*-PEO polymersomes by a previously reported emulsion-centrifugation approach, to create the functional multicompartmentalized structure.[28] PAMO was kept in the lumen of the large PB-*b*-PEO vesicle, because encapsulation in nanoreactors lowered its affinity for the substrate (data not shown). CalB was encapsulated in nanoreactors, because it has been shown previously to remain highly active in this state,[22] and ADH was used either as a cytosolic enzyme or incorporated in PS-*b*-PIAT nanoreactors, to provide a second organelle-bound enzyme.

The PS-*b*-PIAT nanoreactors encapsulating CalB and ADH were prepared and purified according to a previously described procedure,[35] and loading efficiencies of $(21.4 \pm 0.2)\,\%$ (CalB) and $(51.2 \pm 3.2)\,\%$ (ADH) were determined through inductively coupled plasma mass spectrometry measurements (Table S1 in the Supporting Information).[35] The structural integrity of the nanoreactors was verified by transmission electron microscopy (Figure S1 in the Supporting Information), and the size was determined by dynamic light scattering measurements, which yielded average sizes of (187 ± 2) nm with a polydispersity of 0.15 (CalB nanoreactors) and (318 ± 26) nm with a polydispersity of 0.28 (ADH nanoreactors), respectively.

Different cascade reaction mixtures of increasing complexity were first screened in bulk ensemble measurements with fluorescence spectroscopy to obtain reaction conditions that would allow monitoring of the cascade reaction in single functional polymersomes-in-polymersome systems (Figure 2). First, all of the enzymes were used free in solution. These experiments showed that elimination of PAMO from the cascade mixture completely inhibited the reaction, whereas omission of CalB, ADH, or both enzymes severely lowered the speed of the cascade reaction, which demonstrated that all of the enzymes are indeed required for the production of fluorescent resorufin (Figure 2 a). Next, cascade systems were investigated in which first only CalB was encapsulated in nanoreactors and then both CalB and ADH were confined to nanoreactor subcompartments. In this approach, the amounts of enzyme loaded in the nanoreactors were kept the same relative to the concentrations of the free enzymes.

After 24 h at room temperature, the reactions typically reached conversion values ranging from 10–25 %, dependent on the applied conditions. The low reaction rate is likely a result of the different substrate specificities of the enzymes used. However, we still opted for this profluorescent substrate, even if it would be less well accepted by one or more of the enzymes, because fluorescence is the most efficient readout method for our multicompartment system.

Both cascade systems gave a small decrease in the overall reaction speed of 17 and 14 %, respectively, relative to that of the same reaction with the enzymes free in solution (Figure 2 b and Table S2 in the Supporting Information). The slight decrease in reaction rate due to encapsulation could be a result of the encapsulation procedure. In the case of ADH, it can also be attributed to decreased diffusion of the polar cofactor into the nanoreactor.[36] Yet, these results clearly demonstrate that reaction intermediates can easily travel across multiple compartments to react with the different enzymes, which are confined in the cavities.

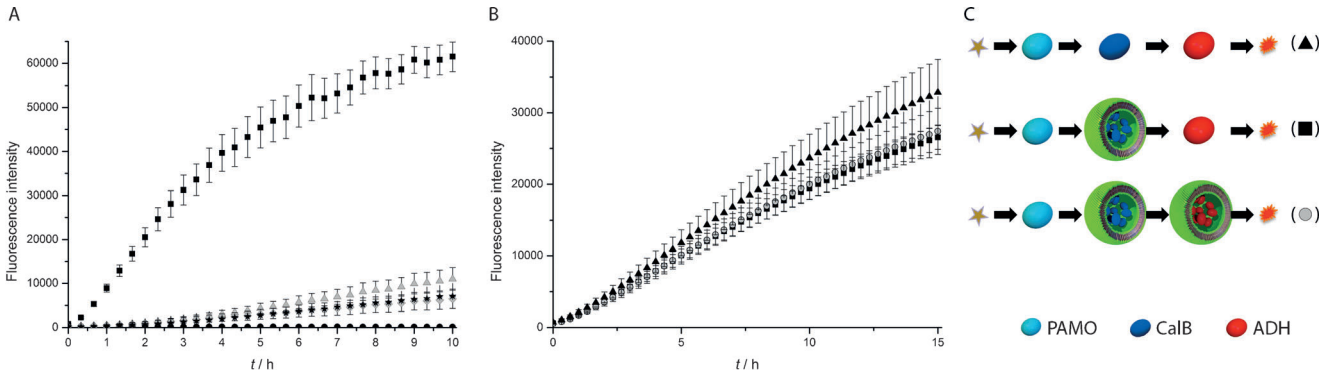

Figure 2. A) Ensemble fluorescence measurements of the cascade reaction at 25 °C, with: 10 μM cytosolic free ADH (■), no CalB (△), no ADH (◇), no CalB and ADH (★), and no PAMO (●). B) Ensemble fluorescence measurements of the cascade reaction with either all of the enzymes in solution (▲), CalB in nanoreactors (■), or CalB and ADH in nanoreactors (○). In all cases, the CalB and ADH concentrations were kept the same, at 0.41 μM and 0.26 μM, respectively. C) Graphical representation of the cascade reactions in (B).

To prove that compartmentalization is a generic strategy for the successful execution of biocatalytic cascade reactions, for which compatibility issues can also occur, we replaced CalB, the enzyme of the second step of the cascade reaction, with alcalase, a protease that shows comparable esterase activity to CalB for certain substrates at room temperature, although its protease activity is more predominant at elevated temperatures (Figure S3 in the Supporting Information). Proteases are, of course, not compatible with other enzymes, because they will degrade any other enzymes present in solution. Yet, if alcalase is encapsulated in a PS-*b*-PIAT nanoreactor (Table S1 and Figure S1 in the Supporting Information), it is physically separated from the other enzymes and should not be able to degrade them, which would thus allow the cascade reaction to take place normally. Alcalase and PS-*b*-PIAT-bound alcalase showed similar rates to that of CalB for the ester hydrolysis reaction at 25 °C (Figure S2a in the Supporting Information). Next, the cascade reaction was performed with alcalase at 37 °C, at which temperature the proteolytic activity is more prominent than at 25 °C (Figure S3 and S4 in the Supporting Information). Clearly, the cascade reaction containing free alcalase was severely inhibited and leveled off much faster than the reaction with CalB (Figure 3a and Table S3 in the Supporting Information), which indicated that degradation of the enzymes is taking place during the cascade reaction. If the PS-*b*-PIAT nanoreactors were used to encapsulate the alcalase, a much smaller effect on the reaction speed was observed, which indicated that compartmentalization of alcalase reduces proteolytic degradation of the other cascade components and, therefore, increases the compatibility of this cascade reaction (Figure 3a and Table S3 in the Supporting Information). The observed decrease in cascade activity for the encapsulated system can be explained by self-degradation of the proteases inside the nanoreactors.

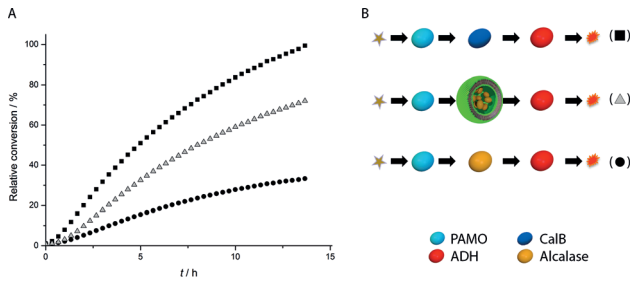

Figure 3. A) Ensemble fluorescence measurements of the cascade reaction at 37 °C, with CalB (■), alcalase (●), or PS-*b*-PIAT-bound alcalase (△) for the ester hydrolysis step. Conversions were normalized based on the maximum conversion of the reaction with CalB. Absolute values are displayed in Figure S5 in the Supporting Information. B) Graphical representation of the utilized cascade systems in (A).

To further demonstrate and analyze the multicompartmentalized nature of this system, the reaction mixture containing free PAMO, CalB- and ADH-loaded polymersomes, substrate, and cofactors was loaded into micrometric PB-*b*-PEO polymersomes by following a previously reported procedure.[28,37] First, an inverted emulsion was created with aqueous droplets of reaction mixture suspended in a solution of toluene; the amphiphilic PB-*b*-PEO was dissolved in the toluene and stabilized the droplet interface. The emulsion droplets were still stable regardless of the higher level of complexity of the aqueous content compared with that in previous reports.[28,37] A fraction of the emulsion was subsequently poured over a biphasic toluene/water interface stabilized by PB-*b*-PEO. Finally, centrifugation of the emulsion droplets through the polymer-stabilized solvent/water interface yielded the "organelle"-containing cell mimics.[28]

Confocal fluorescence microscopy was used to prove that the generation of the final fluorescent reaction product exclusively took place in the cell mimics over time. Numerous vesicles were imaged over time, and the state of the confined reaction at different time points is depicted in Figure 4 and Table S4 in the Supporting Information. Qualitatively, an increase in fluorescence intensity can clearly be observed with time. This was quantitatively demonstrated by the fluorescence-intensity plot profile of vesicle cross-sections for each acquisition shown in Figure 4. At the initial time (t_0), which also corresponds to the negative control without PAMO for longer reaction times, the signal is similar to background intensity, with an average of around 1100 a.u. at any coordinate. At intermediate times (7 h 55 min), there is

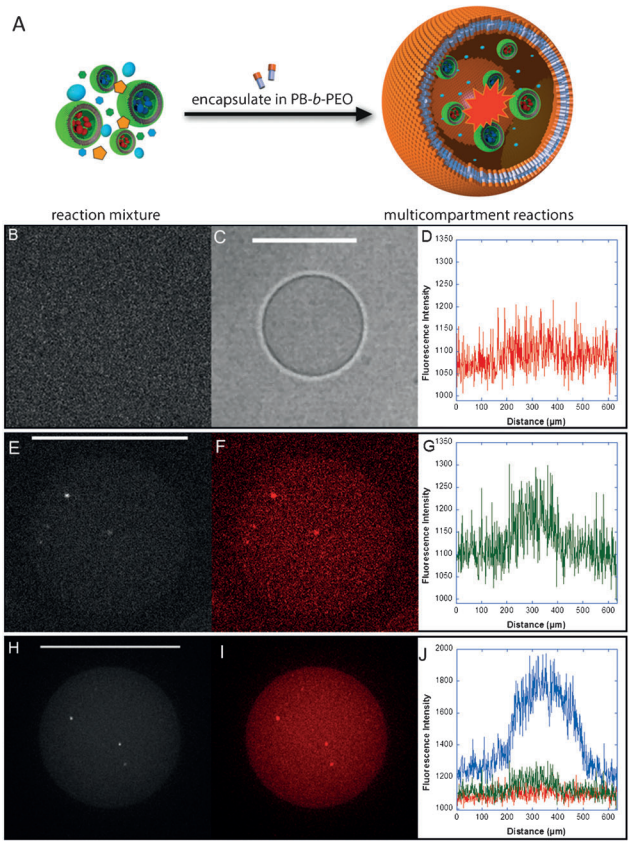

Figure 4. Spinning disk confocal fluorescence micrographs of multicompartmentalized polymersomes. A) Graphical representation of the applied system. B–J) Fluorescence intensity of generated resorufin displayed at initial time (t_0; top), an intermediate time point (7 h 55 min; middle), and after full conversion at 32 h 42 min (t_∞; bottom). Images B, E, and H correspond to the raw acquisitions, which are those that are analyzed in terms of intensity. Image C is observed under bright field. Images F and I are enhanced and colored images for better visualization. The scale bar is C) 20 μm, E) 40 μm, and H) 60 μm. Images D, G, and J are plot profiles of the cross-section for each time point, which demonstrate the drastic increase in fluorescence from the initial background signal to a clear vesicle-based fluorescence signal.

a "bump" rising from the background signal in the profile up to 1250 a.u. intensity. Finally, at full conversion (t_∞), the fluorescence inside the cell mimic has significantly increased up to 1900 a.u. (Figure 4). Table S4 in the Supporting Information displays the average mean intensities and standard errors obtained from five–ten independent multicompartmentalized reactors at these various time points, results that show a significant increase of the fluorescence intensity over time. As shown in Figure S7 in the Supporting Information, which displays all of the confocal acquisitions at the intermediate time point (and in Tables S5–S7 in the Supporting Information, which display all of the numerical data), the mean intensity does not vary with the size of the area. Such results undoubtedly demonstrate that the relative concentration of species is equivalent in all of the cell-mimic reactors, independent of their size, thanks to the quantitative encapsulation of the emulsion-centrifugation process.

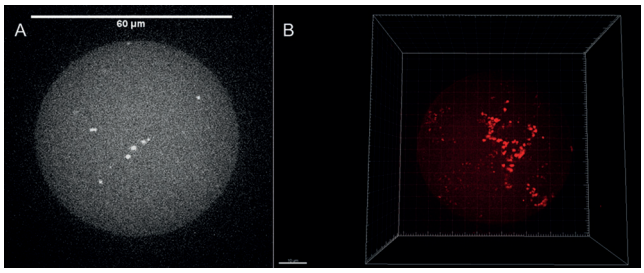

Figure 5. A) Enhanced spinning disk confocal fluorescence micrograph at full conversion of a multicompartmentalized polymersome, obtained with a higher laser power (50% instead of 30%), in order to better highlight the compartmentalized confined fluorescence, because the resorufin is generated in the ADH polymersomes. The scale bar is 60 μm. B) The 3D representation of this full conversion system clearly shows the presence of a large number of such nanosized ADH polymersomes.

Finally, one of the cell mimics at full conversion (t_∞) was reconstructed in 3D to better investigate the location of the final fluorescent product. In Figure 5, both on the 2D confocal acquisition and on this 3D reconstructed vesicle (see also Movie S1 in the Supporting Information for a larger version), the fluorescence clearly appears to be compartmentalized, confined to the inner most compartments. This confinement of the final product is due to the fact that resorufin interacts electrostatically with ADH, the enzyme that enables the last enzymatic reaction step; this interaction prevents fast diffusion of the final fluorescent product from the synthetic organelle. This also indicates that the reactions take place exclusively in the organelle subcompartments, because a homogenously distributed fluorescence was observed for enzymes in solution (Figure S9 in the Supporting Information). Such confinement of fluorophores through electrostatic interactions has been observed previously in PS-*b*-PIAT nanoreactors when a highly charged polymer was included in the particles together with an enzyme.[38] The interaction between ADH and resorufin was further demonstrated by size exclusion chromatography, which only showed coelution of the fluorescent product together with ADH enzymes or ADH nanoreactors (Figure S10 in the Supporting Information).

In conclusion, we have shown that we can construct a structural and functional eukaryotic cell mimic through multicompartmentalization, by loading functional organelle mimics inside larger polymersomes. The concept of enzyme compartmentalization was used to spatially separate incompatible enzymes to retain the functionality of the applied cascade reaction. Furthermore, we applied an original three-enzyme cascade reaction that takes place inside such a scaffold. The cofactor-dependent cascade reaction involved two different enzyme-containing "organelles", as well as a "cytosolic" enzyme. Interestingly, as is particularly visible in 3D-reconstructed cell mimics and by colocalization experiments, the fluorescent end-product seems to be confined mainly in the ADH-containing "organelles" where the production of the final dye takes place.

We anticipate that our multicompartmentalized system can act as a mimic of cellular reaction pathways that take

place in multiple successive compartments and that this system can provide a way to study such cellular processes in more detail. Such research is of fundamental biological and chemical relevance, because investigating how cellular reactions or interactions take place, in biomimetic, confined, and multicompartmentalized architectures, should improve the understanding of how the complexity of the eukaryotic cell is established step by step. Also, in materials chemistry, this level of control over chemical reactions can provide access to powerful new materials; reactions can be truly confined to provide increased efficacy,[39] and incompatible reactions can be separated and therefore conducted simultaneously. As such, miniaturized microreactors should allow control over attoliter or femtoliter volumes and increase safety and efficacy for biocatalysis/bioengineering purposes.

Received: September 16, 2013
Published online: November 19, 2013

Keywords: artificial cells · cascade reactions · enzyme catalysis · nanoreactors · polymersomes

[1] J. W. Szostak, D. P. Bartel, P. L. Luisi, *Nature* **2001**, *409*, 387 – 390.
[2] W. Martin, *Philos. Trans. R. Soc. London Ser. B* **2010**, *365*, 847 – 855.
[3] M. Marguet, C. Bonduelle, S. Lecommandoux, *Chem. Soc. Rev.* **2013**, *42*, 512 – 529.
[4] A. J. Dzieciol, S. Mann, *Chem. Soc. Rev.* **2012**, *41*, 79 – 85.
[5] S. Rasmussen, L. Chen, D. Deamer, D. C. Krakauer, N. H. Packard, P. F. Stadler, M. A. Bedau, *Science* **2004**, *303*, 963 – 965.
[6] V. Noireaux, A. Libchaber, *Proc. Natl. Acad. Sci. USA* **2004**, *101*, 17669 – 17674.
[7] G. Murtas, Y. Kuruma, P. Bianchini, A. Diaspro, P. L. Luisi, *Biochem. Biophys. Res. Commun.* **2007**, *363*, 12 – 17.
[8] K. Kurihara, M. Tamura, K. Shohda, T. Toyota, *Nat. Chem.* **2011**, *3*, 775 – 781.
[9] A. H. Chen, P. A. Silver, *Trends Cell Biol.* **2012**, *22*, 662 – 670.
[10] C. M. Agapakis, P. M. Boyle, P. A. Silver, *Nat. Chem. Biol.* **2012**, *8*, 527 – 535.
[11] J. E. Dueber, G. C. Wu, G. R. Malmirchegini, T. S. Moon, C. J. Petzold, A. V. Ullal, K. L. J. Prather, J. D. Keasling, *Nat. Biotechnol.* **2009**, *27*, 753 – 759.
[12] M. R. Badger, *J. Exp. Bot.* **2003**, *54*, 609 – 622.
[13] A. R. Fernie, F. Carrari, L. J. Sweetlove, *Curr. Opin. Plant Biol.* **2004**, *7*, 254 – 261.
[14] P. Bolinger, D. Stamou, H. Vogel, *Angew. Chem.* **2008**, *120*, 5626 – 5631; *Angew. Chem. Int. Ed.* **2008**, *47*, 5544 – 5549.
[15] L. Hosta-Rigau, S. F. Chung, A. Postma, R. Chandrawati, B. Städler, F. Caruso, *Adv. Mater.* **2011**, *23*, 4082 – 4087.
[16] R. Chandrawati, P. D. Odermatt, S.-F. Chong, A. D. Price, B. Städler, F. Caruso, *Nano Lett.* **2011**, *11*, 4958 – 4963.
[17] L. Hosta-Rigau, O. Shimoni, B. Städler, F. Caruso, *Small* **2013**, *9*, 1 – 11.
[18] O. Kreft, A. G. G. Skirtach, G. B. B. Sukhorukov, H. Möhwald, *Adv. Mater.* **2007**, *19*, 3142 – 3145.
[19] H. Bermudez, A. K. Brannan, D. A. Hammer, F. S. Bates, D. E. Discher, *Macromolecules* **2002**, *35*, 8203 – 8208.
[20] J. Du, R. K. O'Reilly, *Soft Matter* **2009**, *5*, 3544 – 3561.
[21] F. Meng, C. Hiemstra, G. H. M. Engbers, J. Feijen, *Macromolecules* **2003**, *36*, 3004 – 3006.
[22] D. M. Vriezema, P. M. L. Garcia, N. Sancho Oltra, N. S. Hatzakis, S. M. Kuiper, R. J. M. Nolte, A. E. Rowan, J. C. M. van Hest, *Angew. Chem.* **2007**, *119*, 7522 – 7526; *Angew. Chem. Int. Ed.* **2007**, *46*, 7378 – 7382.
[23] J. Gaitzsch, D. Appelhans, L. Wang, G. Battaglia, B. Voit, *Angew. Chem.* **2012**, *124*, 4524 – 4527; *Angew. Chem. Int. Ed.* **2012**, *51*, 4448 – 4451.
[24] C. Nardin, S. Thoeni, J. Widmer, M. Winterhalter, W. Meier, *Chem. Commun.* **2000**, 1433 – 1434.
[25] S. F. M. van Dongen, W. P. R. Verdurmen, R. J. R. W. Peters, R. J. M. Nolte, R. Brock, J. C. M. van Hest, *Angew. Chem.* **2010**, *122*, 7371 – 7374; *Angew. Chem. Int. Ed.* **2010**, *49*, 7213 – 7216.
[26] R. J. R. W. Peters, I. Louzao, J. C. M. van Hest, *Chem. Sci.* **2012**, *3*, 335 – 342.
[27] N. Ben-Haim, P. Broz, S. Marsch, W. Meier, P. Hunziker, *Nano Lett.* **2008**, *8*, 1368 – 1373.
[28] M. Marguet, L. Edembe, S. Lecommandoux, *Angew. Chem.* **2012**, *124*, 1199 – 1202; *Angew. Chem. Int. Ed.* **2012**, *51*, 1173 – 1176.
[29] Z. Fu, M. A. Ochsner, H.-P. M. de Hoog, N. Tomczak, M. Nallani, *Chem. Commun.* **2011**, *47*, 2862 – 2864.
[30] S.-H. Kim, H. C. Shum, J. W. Kim, J.-C. Cho, D. A. Weitz, *J. Am. Chem. Soc.* **2011**, *133*, 15165 – 15171.
[31] H.-C. Chiu, Y.-W. Lin, Y.-F. Huang, C.-K. Chuang, C.-S. Chern, *Angew. Chem.* **2008**, *120*, 1901 – 1904; *Angew. Chem. Int. Ed.* **2008**, *47*, 1875 – 1878.
[32] D. E. Torres Pazmiño, A. Riebel, J. de Lange, F. Rudroff, M. D. Mihovilovic, M. W. Fraaije, *ChemBioChem* **2009**, *10*, 2595 – 2598.
[33] M. C. Gutiérrez, A. Sleegers, H. D. Simpson, V. Alphand, R. Furstoss, *Org. Biomol. Chem.* **2003**, *1*, 3500 – 3506.
[34] S. Pautot, B. J. Frisken, D. A. Weitz, *Langmuir* **2003**, *19*, 2870 – 2879.
[35] S. F. M. van Dongen, M. Nallani, J. J. L. M. Cornelissen, R. J. M. Nolte, J. C. M. van Hest, *Chem. Eur. J.* **2009**, *15*, 1107 – 1114.
[36] S. A. Meeuwissen, A. Rioz-Martínez, G. de Gonzalo, M. W. Fraaije, V. Gotor, J. C. M. van Hest, *J. Mater. Chem.* **2011**, *21*, 18923 – 18926.
[37] M. Marguet, O. Sandre, S. Lecommandoux, *Langmuir* **2012**, *28*, 2035 – 2043.
[38] M. Nallani, R. Woestenenk, H.-P. M. de Hoog, S. F. M. van Dongen, J. Boezeman, J. J. L. M. Cornelissen, R. J. M. Nolte, J. C. M. van Hest, *Small* **2009**, *5*, 1138 – 1143.
[39] Q. Chen, H. Schonherr, G. Julius Vancso, *Small* **2009**, *5*, 1436 – 1445.

